Supporting Information

Influence of Morphology of Monolithic Sulfur-Poly(acrylonitrile) Composites Used as Cathode Materials in Lithium-Sulfur Batteries on Electrochemical Performance

Tim Lebherz[a,b], Martin Frey[c], Andreas Hintennach[b], Michael R. Buchmeiser*[a,d]

[a] Institute of Polymer Chemistry, University of Stuttgart, 70569 Stuttgart, Germany

[b] Daimler AG, RD/EBZ, HPC G012-BB, 71034 Böblingen, Germany

[c] Daimler AG, RD/EBB, HPC X461, 71059 Sindelfingen, Germany

[d] German Institutes of Textile and Fiber Research (DITF) Denkendorf, 73770 Denkendorf, Germany

Nitrogen desorption/adsorption measurements

The specific surface area (BET-method, multipoint determination) and pore size distributions (BJH-method) were determined via nitrogen adsorption/desorption using an *Autosorb-1* gas sorption analyzer from *Quantachrome*. All samples were degassed for 20 hours at 85 °C under vacuum before characterization.

Table S1: Specific surface areas, average pore sizes and pore volumina of monoliths **PAN-1 – PAN-6** determined by N_2-adsorption.

	specific surface area [$m^2 \cdot g^{-1}$]	**average pore diameter** [nm]	**pore volume*** [$cm^3 \cdot g^{-1}$]
PAN-1	28	47	0.19
PAN-2	30	30	0.22
PAN-3	22	32	0.17
PAN-4	24	41	0.26
PAN-5	225	43	2.45
PAN-6	106	44	1.18

*for pores smaller than 300 nm, measured at $p/p_0 = 0.99$.

Isotherms of the SPAN-monoliths

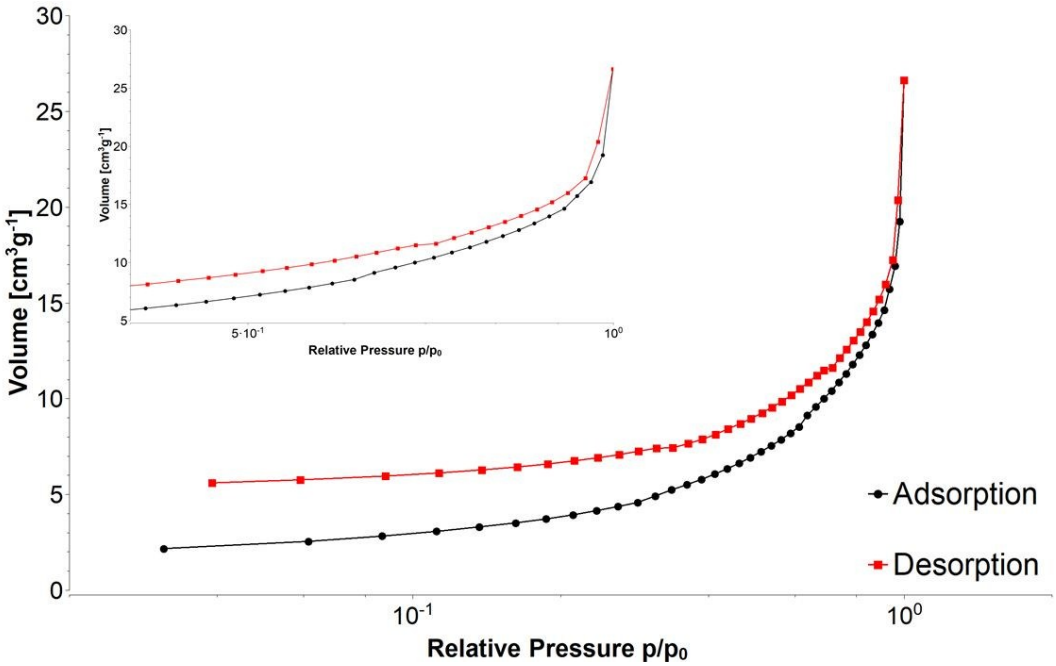

Figure S1: Sorption isotherm of the monolith **SPAN-1** as a result of the N_2-adsorption/desorption measurements, x-axis in logarithmic scale.

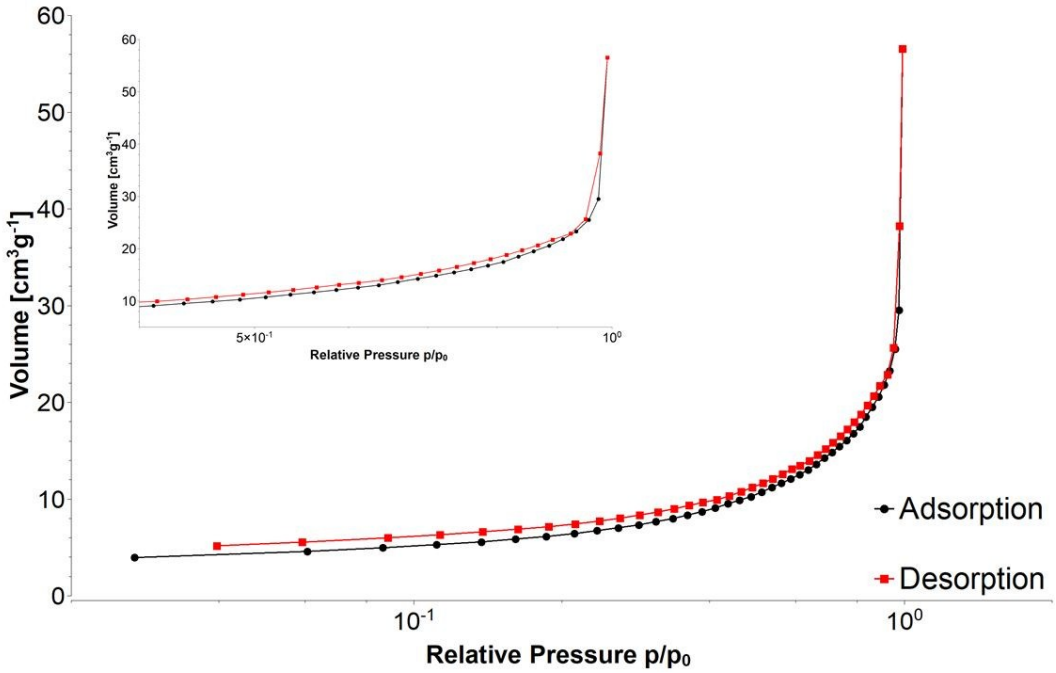

Figure S2: Sorption isotherm of the monolith **SPAN-2** as a result of the N_2-adsorption/desorption measurements, x-axis in logarithmic scale.

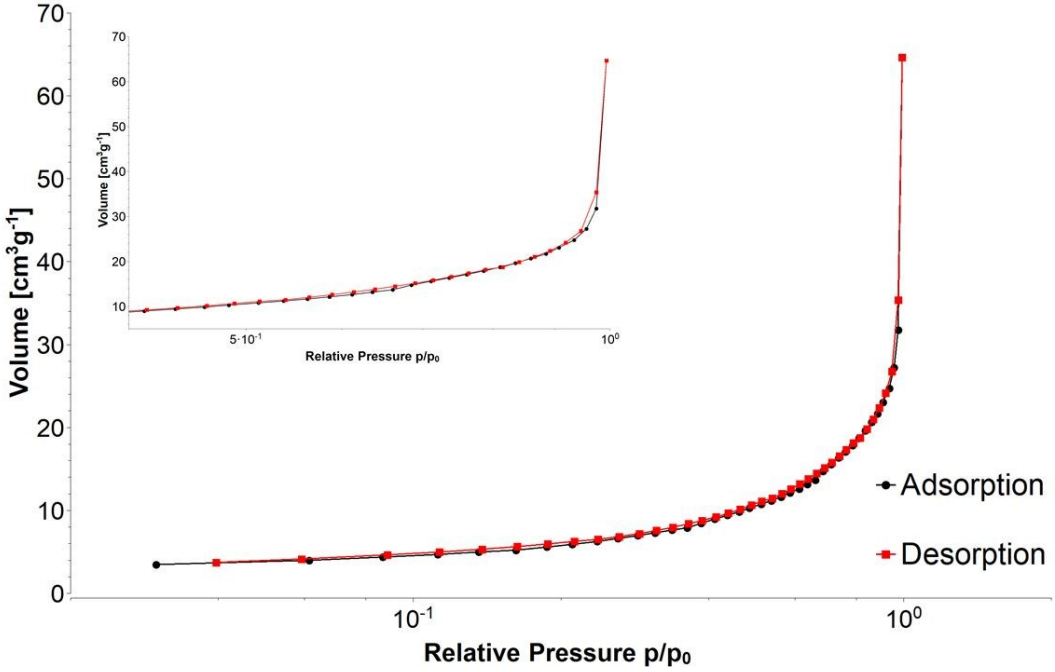

Figure S3: Sorption isotherm of the monolith **SPAN-3** as a result of the N_2-adsorption/desorption measurements, x-axis in logarithmic scale.

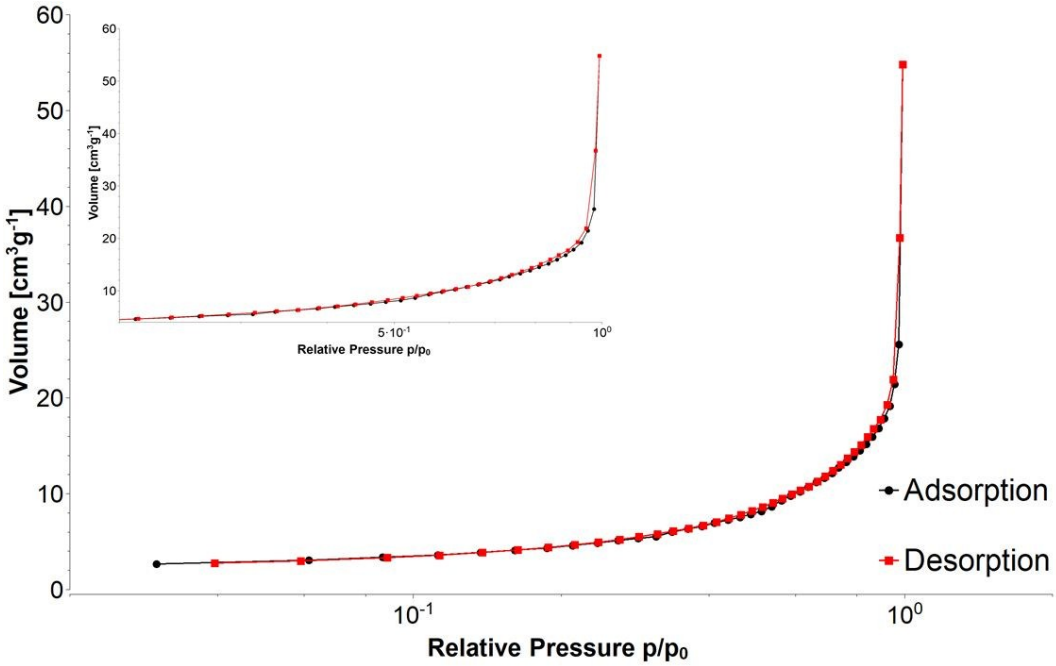

Figure S4: Sorption isotherm of the monolith **SPAN-4** as a result of the N_2-adsorption/desorption measurements, x-axis in logarithmic scale.

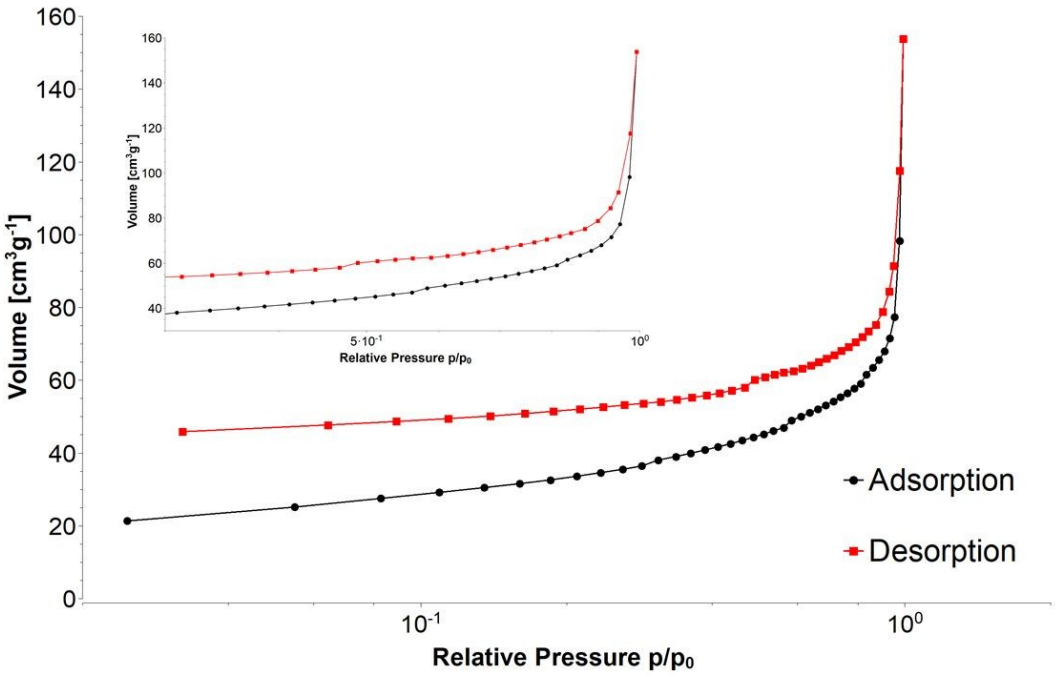

Figure S5: Sorption isotherm of the monolith **SPAN-5** as a result of the N_2-adsorption/desorption measurements, x-axis in logarithmic scale.

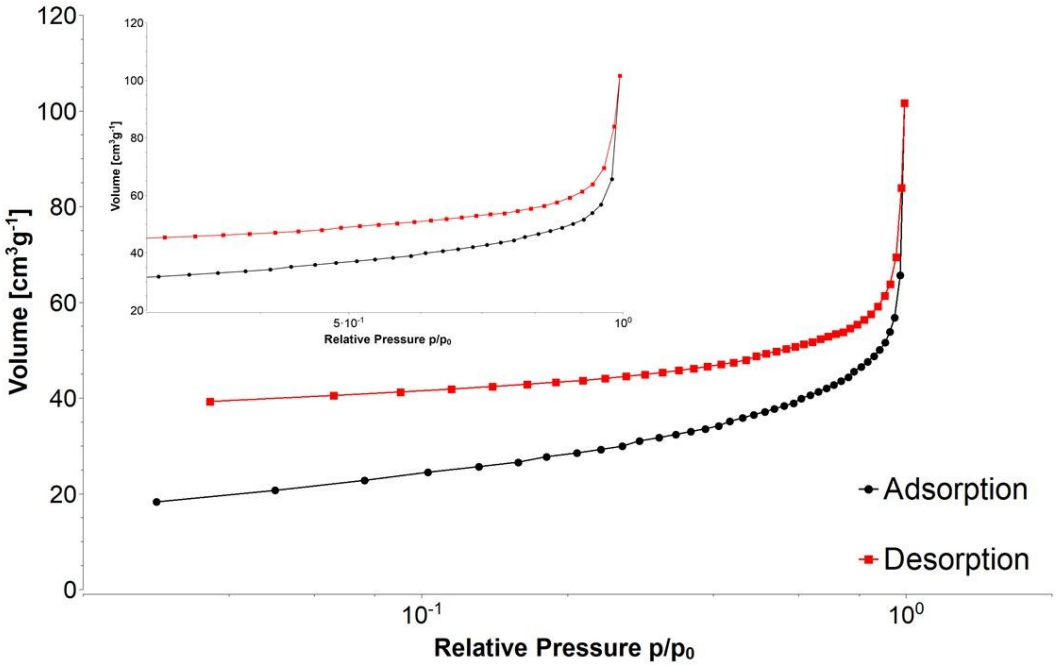

Figure S6: Sorption isotherm of the monolith **SPAN-6** as a result of the N_2-adsorption/desorption measurements, x-axis in logarithmic scale.

Pore size distributions of the SPAN-monoliths

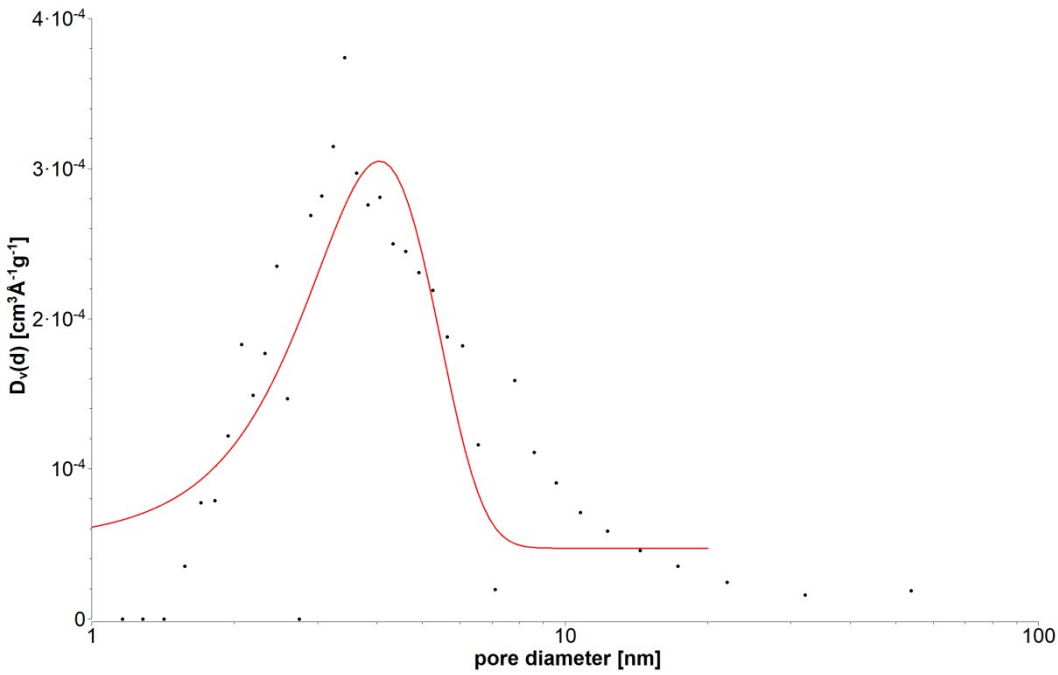

Figure S7: Pore size distribution of **SPAN-1** (with Gaussian fit).

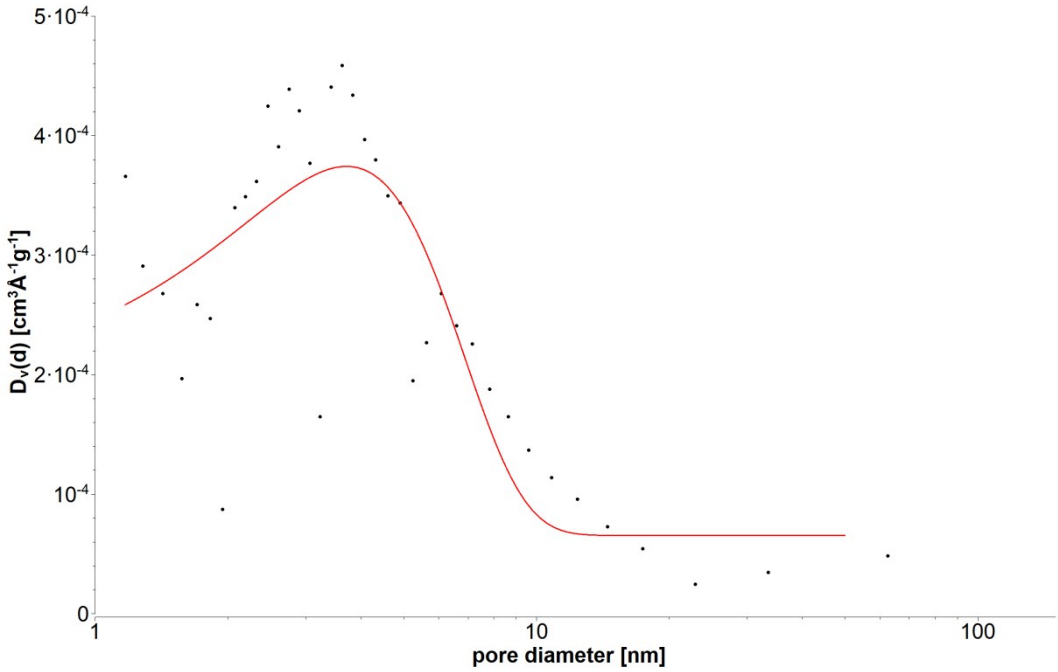

Figure S8: Pore size distribution of **SPAN-2** (with Gaussian fit).

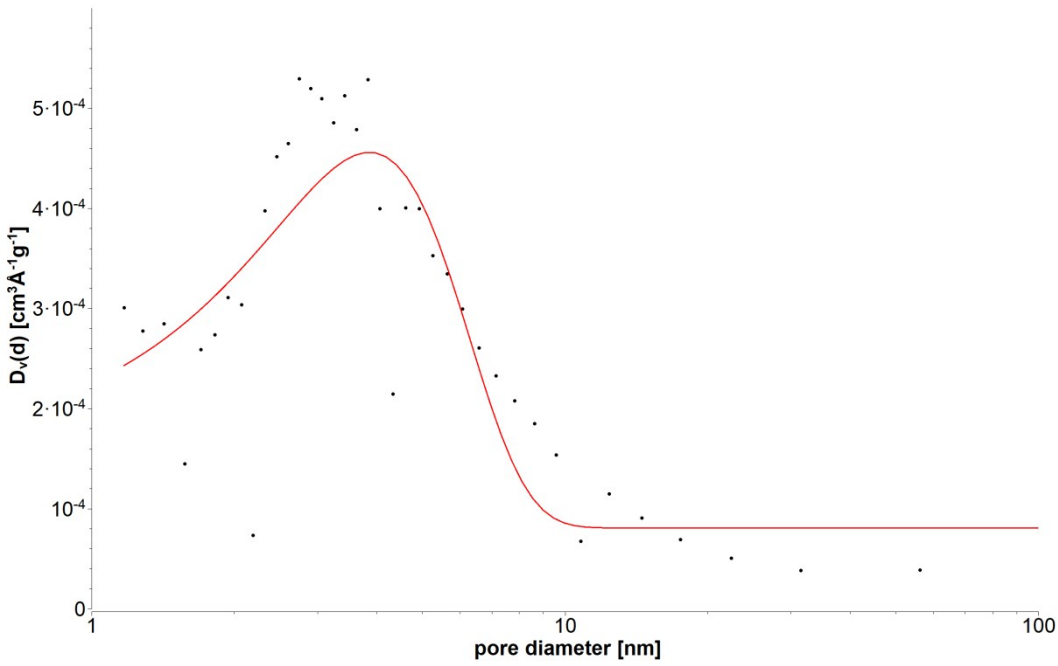

Figure S9: Pore size distribution of **SPAN-3** (with Gaussian fit).

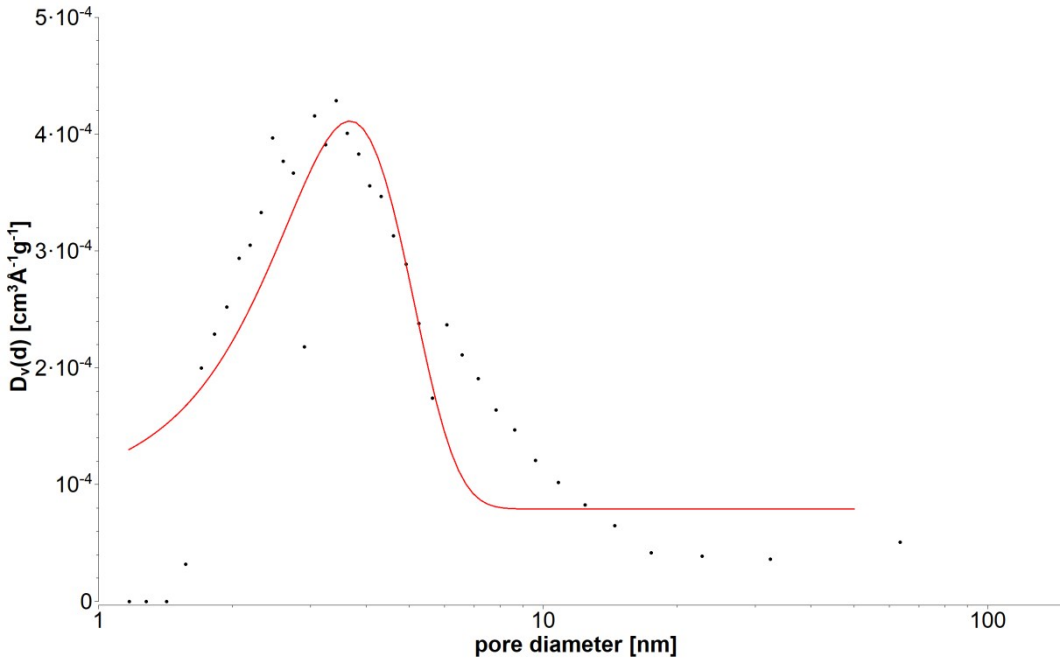

Figure S10: Pore size distribution of **SPAN-4** (with Gaussian fit).

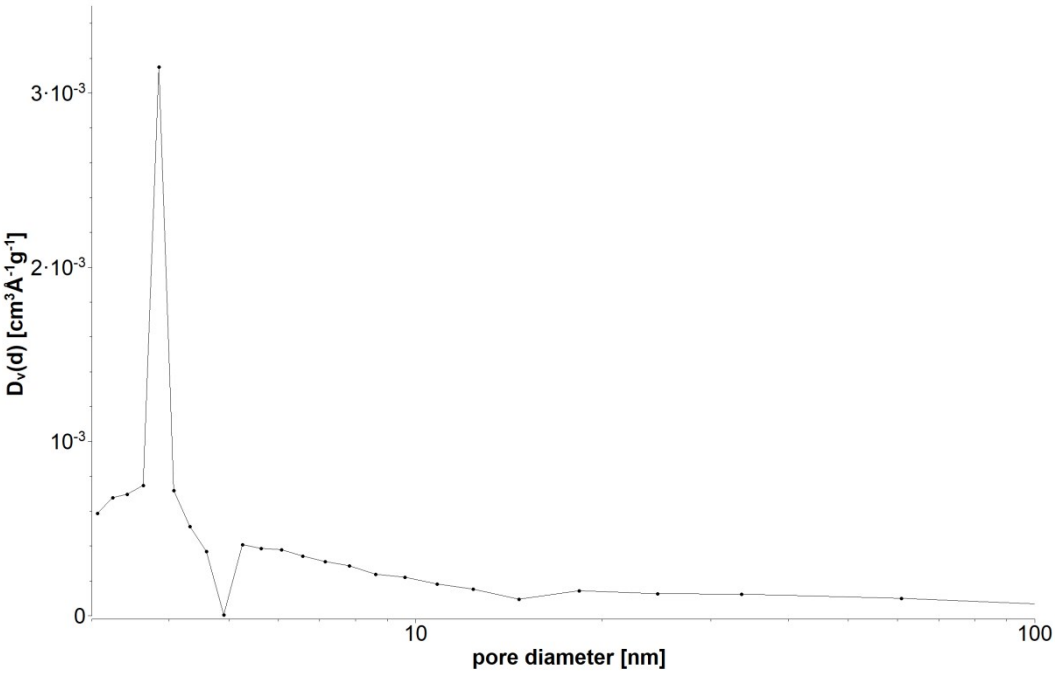

Figure 11: Pore size distribution of **SPAN-5**.

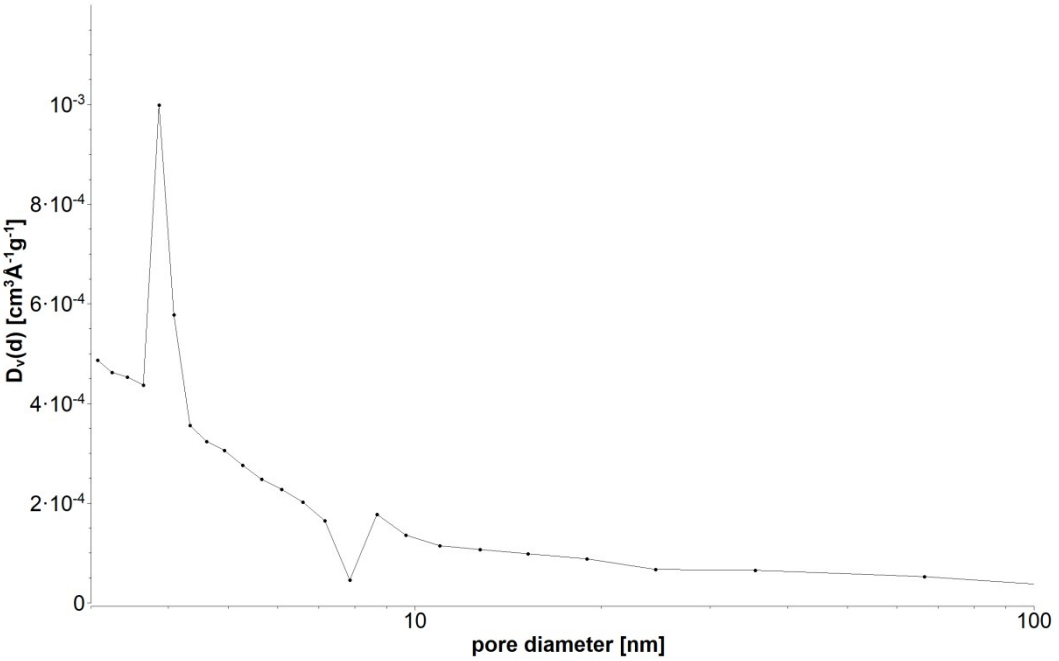

Figure S12: Pore size distribution of **SPAN-6**.

Mercury intrusion

The interparticle void volumes and the average diameters of the interparticle voids of the SPAN-materials were determined via mercury intrusion, which was carried out on a *POREMASTER 60-GT* (3P INSTRUMENTS GmbH & Co. KG in Odelzhausen, Germany). All samples were degassed for 3 hours at 80 °C before characterization.

Table S2: Interparticle void volumes and average sizes of the interparticle voids of the synthesized SPAN-monoliths **SPAN-1 - SPAN-6**.

	average diameter of the interparticle voids [nm]	**interparticle void volume [$cm^3 \cdot g^{-1}$]**
SPAN-1	180	0.21
SPAN-2	390	0.68
SPAN-3	420	0.71
SPAN-4	470	0.80
SPAN-5	470	2.10
SPAN-6	150	0.78

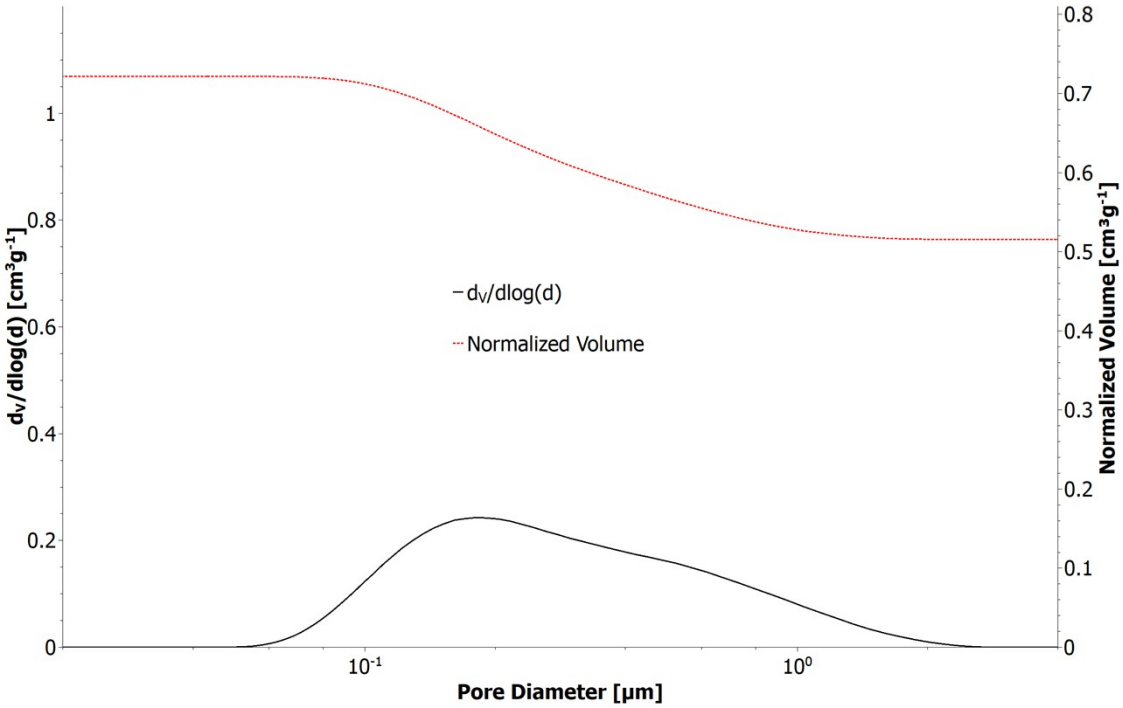

Figure S13: Pore size distribution determined via mercury porosimetry of **SPAN-1**.

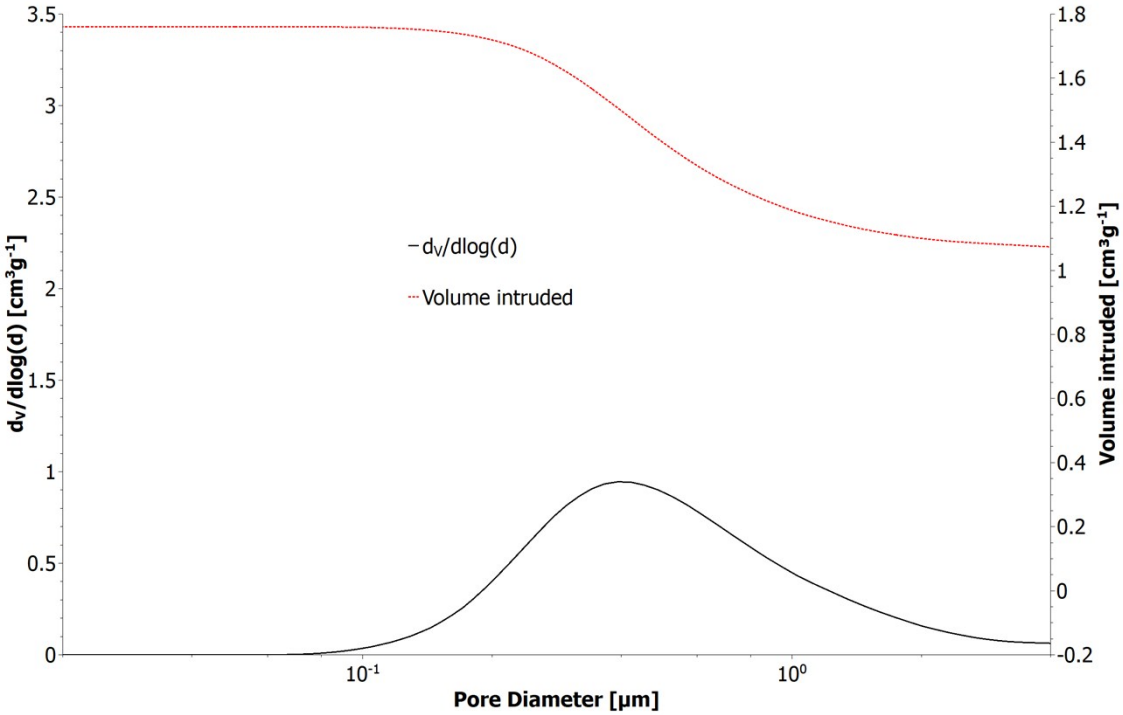

Figure S14: Pore size distribution determined via mercury porosimetry of **SPAN-2**.

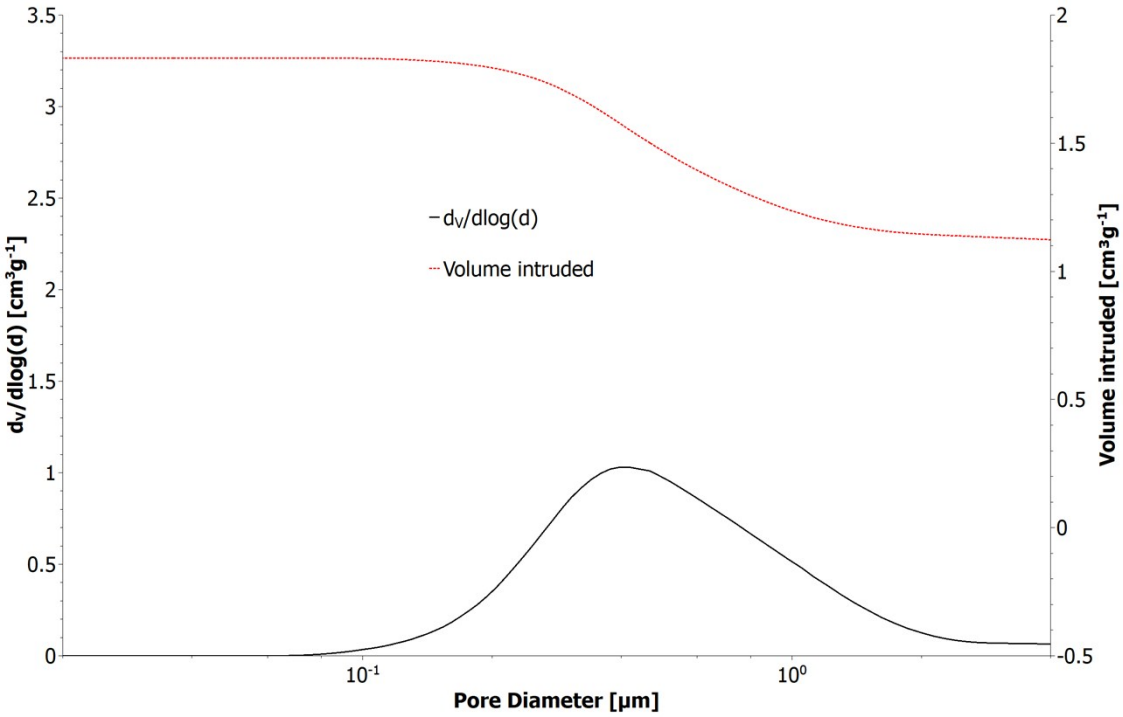

Figure S15: Pore size distribution determined via mercury porosimetry of **SPAN-3**.

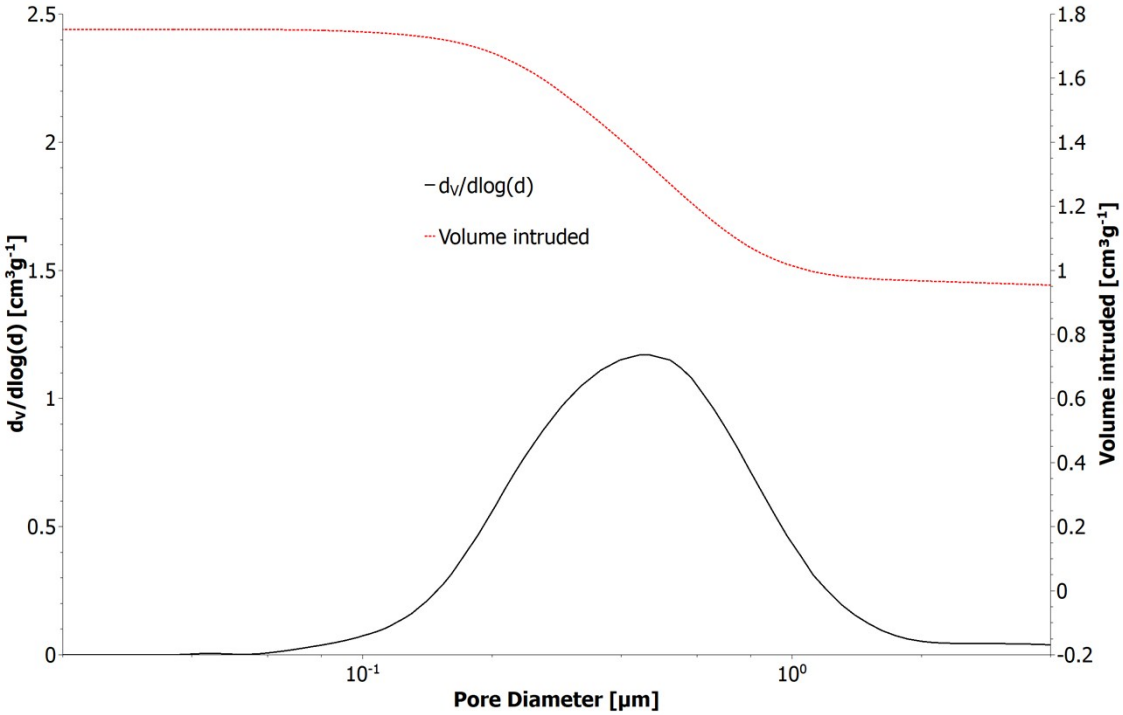

Figure S16: Pore size distribution determined via mercury porosimetry of **SPAN-4**.

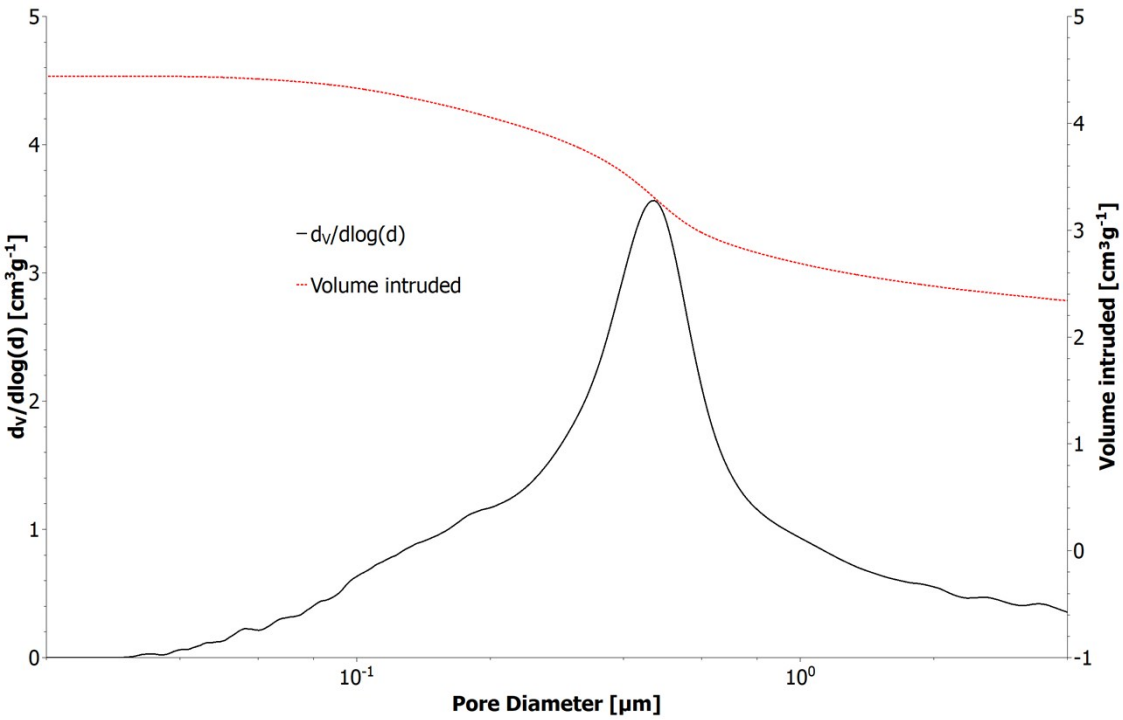

Figure S17: Pore size distribution determined via mercury porosimetry of **SPAN-5**.

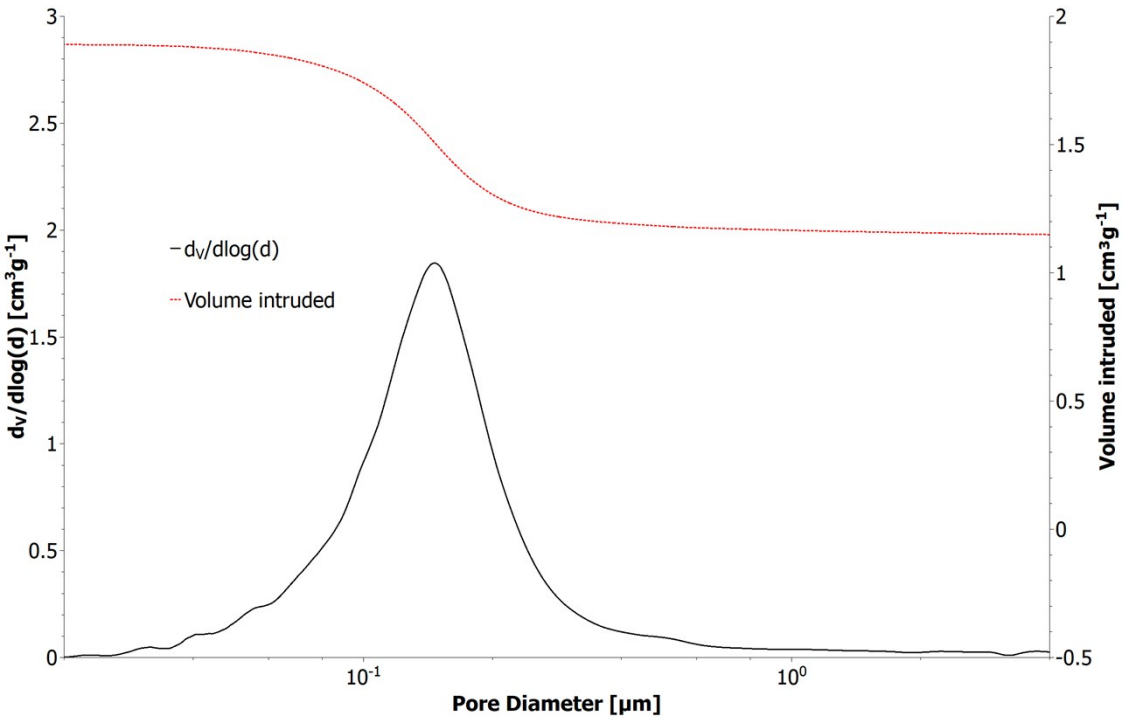

Figure S18: Pore size distribution determined via mercury porosimetry of **SPAN-6**.

SEM pictures of SPAN-monoliths

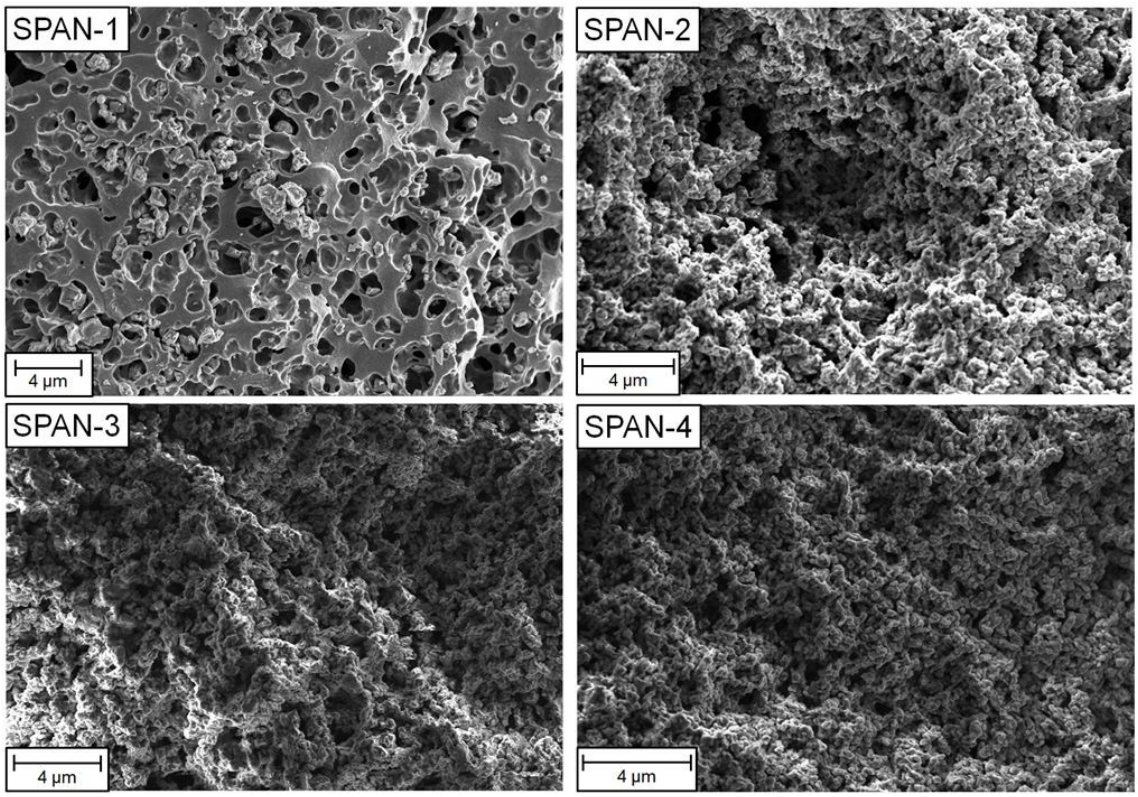

Figure S19: SEM-pictures of the SPAN-monoliths **SPAN-1** - **SPAN-4**.

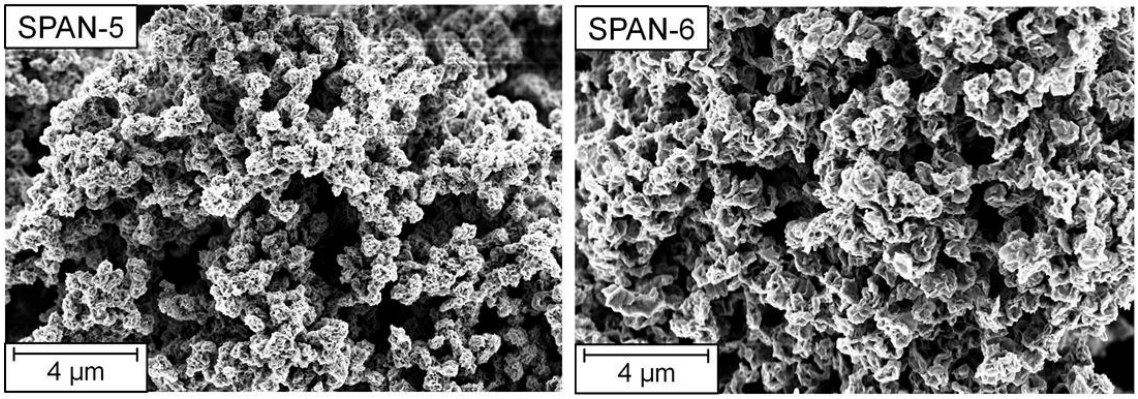

Figure S20: SEM-pictures of the SPAN-monoliths **SPAN-5** and **SPAN-6**.

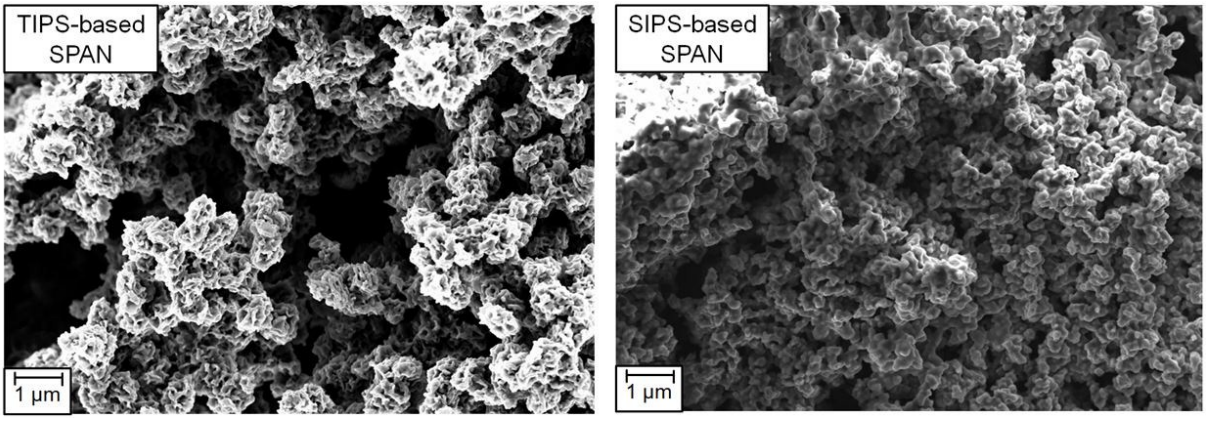

Figure S21: Comparison of the structure of a TIPS-based SPAN-monolith and a SIPS-based SPAN-monolith with a larger magnification.

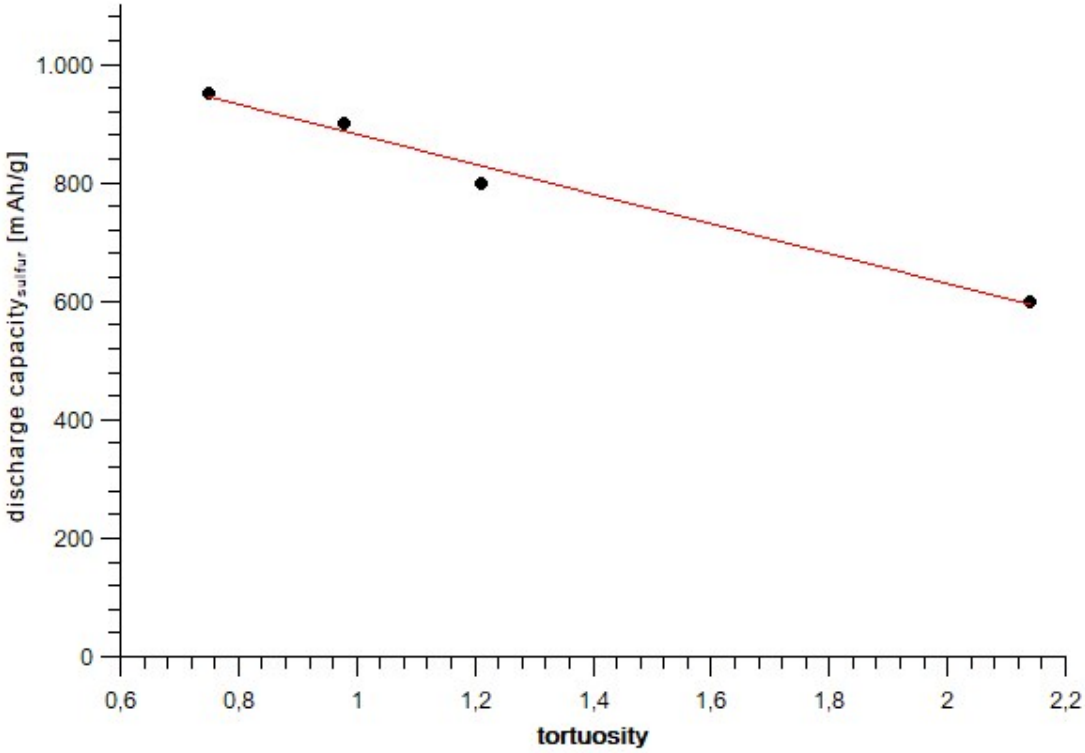

Figure S22: Correlation between tortuosity and the specific discharge capacity$_{sulfur}$ at 1 C (at cycle 30) of **SPAN 1-4**.

IR-spectroscopy

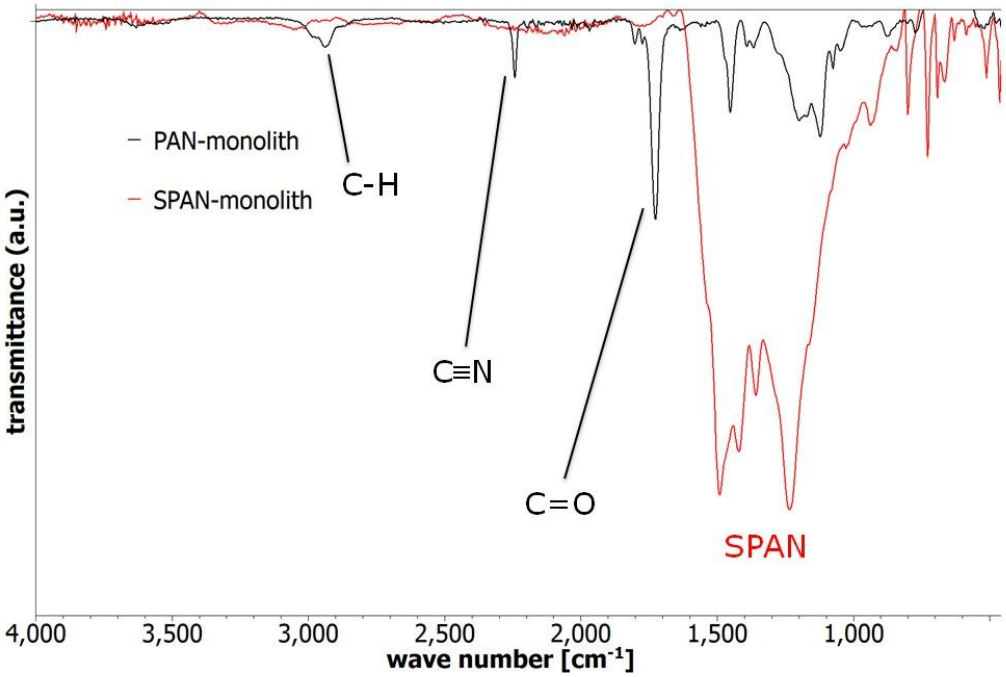

Figure S23: Representative IR-spectrum of SIPS-derived monolith **PAN-4** (black) and monolithic **SPAN-4** (red) The IR-spectra of all other SIPS-derived (S)PAN-monoliths looked similar.

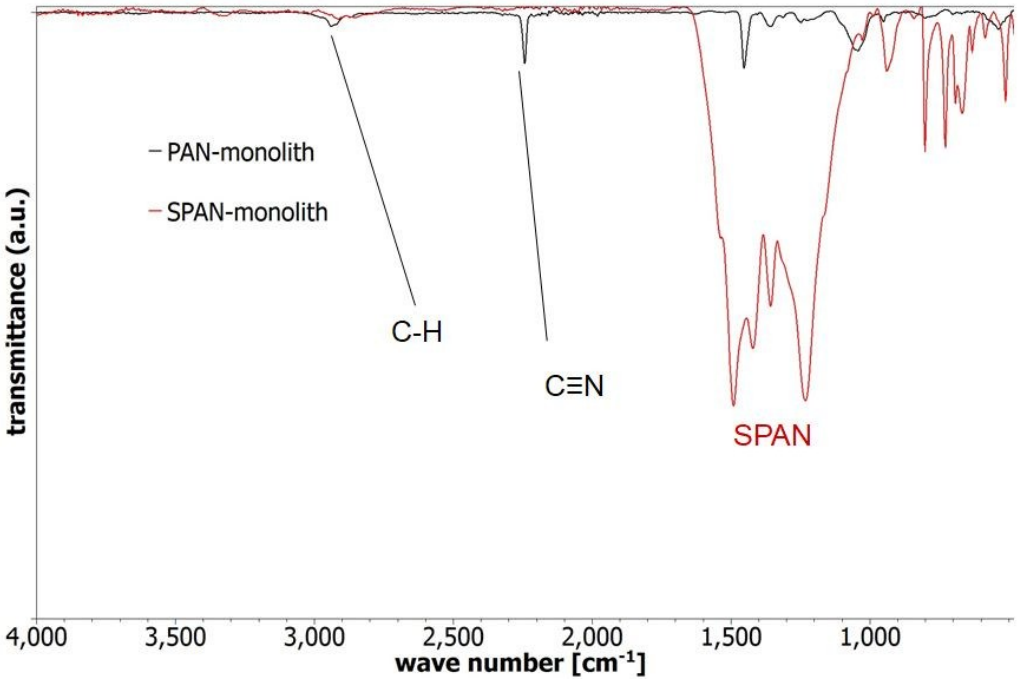

Figure S24: Representative IR-spectrum of TIPS-derived monolith **PAN-5** (black) and monolithic **SPAN-5** (red), The IR-spectra of all other TIPS-derived (S)PAN-monoliths looked similar.

Electrochemistry

Cyclovoltammetry: All cells were first charged at 0.1 C until a voltage of 3 V was reached. Cyclovoltamograms were recorded in a range of 1 to 3 V with a slope of 0.05 mV/s.

Symmetrical Stress Test

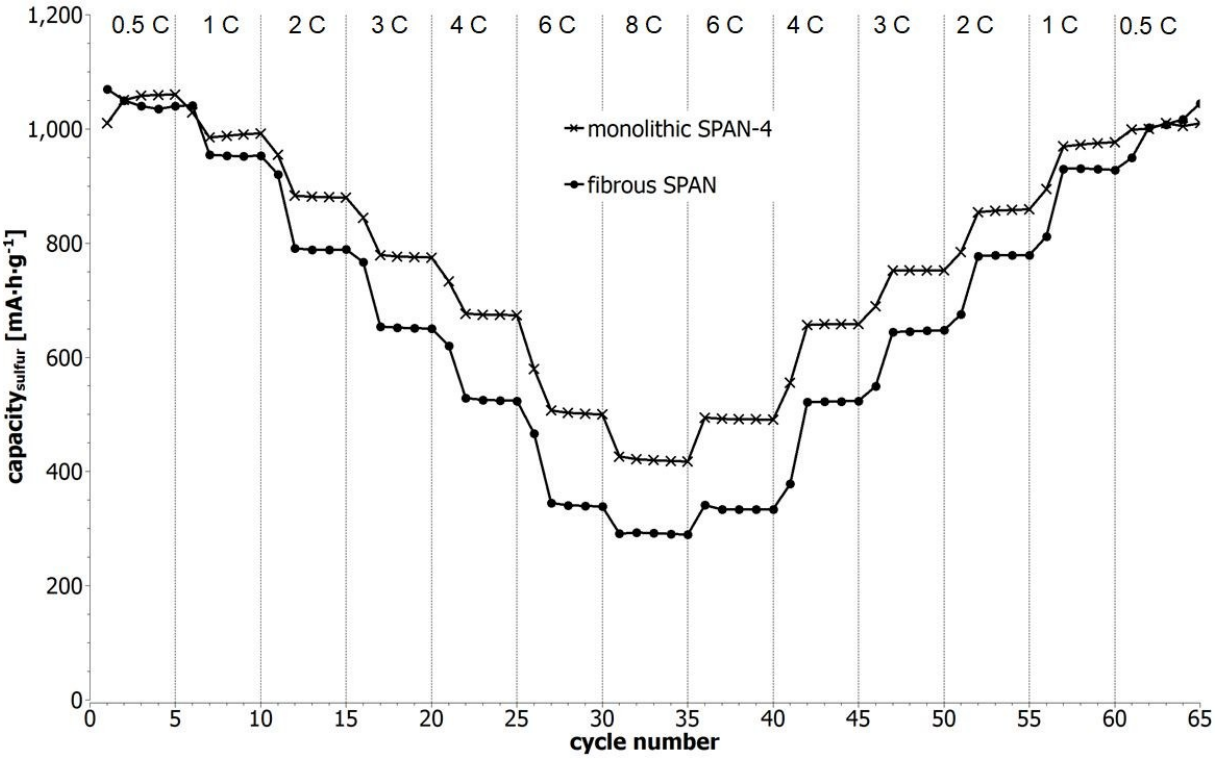

Figure S25: Symmetrical stress test 0.5 C - 1 C - 2 C - 3 C - 4 C - 6 C - 8C of a cell using monolith **SPAN-4** as active material and results of a cell using fibrous SPAN as active material for comparison.

Four Point Resistivity Measurements (van der Pauw Method)

Cathodes: Resistivity was measured on a *Sigmatone H-100 Probe Station*; a Keithley *SourceMeter 2636B* was used as electric current source. For resistivity measurements of the cathode coatings, the coating was removed from the current collector and coated on a non-conducting *Mylar* foil.

Table S3: Specific electronic conductivities of the cathode coatings based on monolithic **SPAN 1 – 6** as active material.

	specific electronic conductivity (cathodes) [S·cm^{-2}]
SPAN-1	0.16
SPAN-2	0.072
SPAN-3	0.069
SPAN-4	0.074
SPAN-5	0.016
SPAN-6	0.050

Monolithic SPAN: Monolithic SPAN-materials were pressed into pellets, which were then electrically contacted via four gold pins in a custom-made cell set-up connected to a *Keithley MultiMeter 2700.* The conductivity of all monolithic SPAN-materials was < 10^{-8} S·cm^{-1}.